https://doi.org/10.5194/gchron-2020-22
Preprint. Discussion started: 27 July 2020

The use of ASH-15 flowstone as a matrix-matched reference material for laser-ablation U-Pb geochronology of calcite

Perach Nuriel[1], Jörn-Frederik Wotzlaw[2], Maria Ovtcharova[3], Anton Vaks[1], Ciprian Stremtan[4], Martin Šala[5], Nick M. W. Roberts[6], and Andrew R. C. Kylander-Clark[7]

[1] Geological Survey of Israel, 32 Yeshayahu Leibowitz St. Jerusalem, 9692100, Israel

[2] Institute of Geochemistry and Petrology, ETH Zurich, Clausiusstrasse 25 I CH-8092 Zurich, Switzerland

[3] Department of Earth Sciences, University of Geneva, Geneva, Switzerland

[4] Teledyne Photon Machines, 384 Gallatin Park Drive, Bozeman, MT 59715, USA

[5] Department of Analytical Chemistry, National Institute of Chemistry, Hajdrihova 19, SI-1000 Ljubljana, Slovenia.

[6] Geochronology and Tracers Facility, British Geological Survey, Environmental Science Centre, Nottingham, NG12 5GG, UK

[7] Department of Earth Science, University of California, Santa Barbara, CA 93106, USA.

Abstract

Latest advances in laser ablation inductively coupled plasma mass spectrometer (LA-ICPMS) allow for accurate *in-situ* U-Pb dating of carbonate material, with final age uncertainties usually >3% 2σ. Cross-laboratory reference materials (RMs) used for sample-bracketing are currently limited to WC1 calcite with an age of 254.4 ± 6.5 (2σ). The minimum uncertainty on any age determination with the LA-ICPMS method is therefore ≥ 2.5%, and validation by secondary RMs ~~are~~ usually performed on in-house standards. This contribution present a new reference material, ASH-15, a flowstone that is dated here by high-precision Isotope Dilution (ID) TIMS analysis using 36 sub-samples, 1-7 mg each. Age results presented here are slightly younger compared to previous ID dating of ASH-15, but in agreement with *in-situ* analyses (using WC1 as a RM). We provide new correction parameters to be used as primary or secondary standardization. The suggested $^{238}U/^{206}Pb$ apparent age, not corrected for disequilibrium and without common-lead anchoring, is 2.965 ± 0.011 Ma (2σ). The new results could improve the propagated uncertainties on the final age with a minimal value of 0.4%, which is approaching the uncertainty of typical ID analysis on, for example, zircon (<1% 2s). We show that although LA-ICPMS spot analyses of ASH-15 exhibit~~s~~ significant scatter in their isotopic ratios, the down-hole fractionation of ASH-15 is similar to that of other reference materials. ~~For LA work, we recommend the use of the new ID-TIMS ages that are 1.3-1.5% younger than previously suggested, because of the lower uncertainties (0.4%), the large number of sub-samples (n=36), the use of the EARTHTIME isotopic tracers, and the small aliquots (1-7 mg) that are more representative of laser-ablation spot analysis.~~

1. Introduction

Recent advances in laser ablation techniques applied to multi-phase carbonates allow for accurate dating of a variety of sample types, including calcite cements (Li et al., 2014; Godeau et al., 2018; Anjiang et al., 2019; Holdsworth et al., 2019), hydrothermal veins (Coogan et al., 2016; MacDonald et al., 2019; Piccione et al., 2019), fault-related veins, breccia cement, and slickenfibers (Ring and Gerdes, 2016; Roberts and Walker, 2016; Nuriel et al., 2017; Hansman et al., 2018; Parrish et al., 2018; Nuriel et al., 2019), and speleothems (Woodhead and Petrus, 2019). With increasing attention ~~on~~ climatic, seismic, and environmental events in the geological record there is a growing need for dating techniques that can be accurate~~ly~~ and easily implemented ~~to~~ samples at the sub-millimeter scale. This newly emerging technique has the potential to contribute to our understanding of the duration, rate, and extent of these important events in the geological record.

The *in-situ* approach has a great research potential for studying texturally complex samples because it can resolve problems of age mixing of different phases or averaging of continuous growth at the sub-millimeter scale, and thus increase the overall accuracy of the dated material. While the precision of traditional isotope-dilution (ID) U-Pb analyses is still favorable (<1% 2σ) (Woodhead and Petrus, 2019), increasing analytical development of the LA-ICPMS method indicates the potential for improving the currently reported uncertainties (usually >3% 2σ). Finding the right matrix-matched reference material (RM) is a major hurdle for LA analyses of carbonates because of the variety of mineralogy (calcite, dolomite, and aragonite), textures, composition (e.g. high-magnesium calcite, high common-lead), and ages (e.g. low radiogenic lead in young samples). Textural differences such as microcrystalline, fine- and coarse-grained material, between the unknown and RMs can contribute to high uncertainties due to differences in ablation efficiency, down-hole fractionation, and differences in crater morphology (e.g. Guillong et al., 2020 and Elisha et al, 2020, this issue). Observed deviations are potentially up to 20% of the final intercept age depending on the degree of crater geometry mismatch and are related to either to downhole fractionation and/or matrix effects (Guillong et al., 2020).

Currently, the most commonly used procedure for mass-bias correction in the LA method, is by standard-sample bracketing. For this, the ^{238}U/^{206}Pb LA-age of the RMs is corrected to the true RM's ^{238}U/^{206}Pb apparent age (not corrected for disequilibrium) as measured independently by an ID method (e.g. ID-TIMS). The RMs are measured throughout each session along with the unknown samples, and a normalization factor is applied to correct both the RMs and the unknowns. Uncertainty propagation onto the age of the unknowns includes the uncertainties of the 'true' RM age. As a result, the accuracy of the LA analyses can only be as good as the uncertainties on the age of the RMs which is by itself subjected to analytical challenges due to natural heterogeneities, impurities, and textural complexities at the submillimetre scale. It is therefore essential that the 'true age' of the reference material will reflect these complexities while maintaining minimal uncertainties.

Currently, several in-house standards are being used as reference materials, including Duff Brown Tank (64 Ma; Hill et al., 2016), and JT (13.797 ± 0.031 Ma; Guillong et al., 2020). The only well-characterized reference material that is distributed across laboratories is the WC1 calcite with an age of 254.4 ± 6.5 2s (2.5%) (Roberts et al., 2017). The use of WC1 alone for mass-bias correction has several disadvantages. First, it is highly recommended with all in situ U-Th-Pb geochronology to use secondary RMs to validate any correction parameters that are being used, and to appropriately propagate uncertainties. Second, the relatively high uncertainty (2.5%) on the age of WC1 sets a minimal uncertainty on any LA U-Pb age determination. Finally, the quantity of the WC1 sample that is currently available for future work is limited and is likely to not fully meet the growing demands of the LA scientific community; although, we note here that there is a potential for further sample collection from the original site.

This contribution introduces a new carbonate reference material that can be widely used for *in-situ* dating of calcite as primary or as cross-reference material with other available standards. We characterise the reference material at various resolutions using a combination of (1) laser ablation imaging (20 µm square beam); (2) LA spot analysis, ~80-110 µm in diameter, conducted on both multi-collector (MC) and single collector inductively coupled plasma mass spectrometer (ICPMS); and (3) ID-TIMS analyses of 36 sub-samples ~1-7 mg aliquots. We discuss several key issues related to the use of ASH-15 sample as a RM, including down-hole fractionation, heterogeneities, previous bulk analyses, and the possible effect of samples size and blank corrections, to provide the best correction parameters and suggested protocols for users of the LA scientific community.

2. The ASH-15 flowstone

The ASH-15 flowstone was found in Ashalim Cave, a karstic cave in the central Negev Desert (30°56′36.2″ N, 34°44′22.5″ E), southern Israel, which is part of the northern margin of the Saharan–Arabian desert belt. The cave entrance is located at an elevation of 414 m above sea level and 67 km SE from the Mediterranean Sea coast. The cave is a three-dimensional hypogene maze with a total length of 540 m, situated in Turonian limestone rock strata, at depths of 0-31 m below the surface. The cave is richly decorated with vadose speleothems, such as stalagmites, stalactites and flowstone, which are not active today because of the aridity of the climate in the area (Vaks et al, 2010, 2018), but periods of their deposition correspond to past episodes of wet climate in present-day desert The thickness of the speleothems varies from several cm to a few tens of cm. The soil above the cave is silicate loess, originated mainly from aeolian dust (Crouvi et al., 2010) and the present day vegetation is composed of sparse xeric shrubs with <10% vegetation cover.

The vadose speleothems of Ashalim Cave are composed of low-Mg calcite, and are divided into a relatively thick Pliocene Basal layer, and thinner Pleistocene layers above it. The Basal layer varies from 5 to 25 cm in thickness and comprises c. 90% of the speleothem volume in the cave. It is composed of massive yellow calcite crystals (Fig. 1a-b), often showing continuous growth in stalagmites and flowstone, suggesting deposition from continuously dripping water. In all speleothems the Basal layer is terminated at its top by a <1 mm layer of microcrystalline calcite, evaporite minerals and reddish clays (Fig. 1a), that is interpreted as a hiatus (growth break) separating the Basal Pliocene layer and Quaternary layers above it (Vaks et al., 2013). The thickness of Pleistocene top layers varies from several mm to 17 cm, but usually does not exceed a few cm, comprising about 10% of the speleothem volume in the cave. It is composed of alternating layers of brown calcite, with the youngest top layer (where found) composed of yellow calcite. Several variably colored layers <1 mm thick of microcrystalline calcite, evaporite minerals and reddish clays are found within the columnar crystalline structure, suggesting hiatuses in speleothem deposition (Vaks et al., 2013).

The youngest periods of speleothem deposition in several Ashalim Cave speleothems were dated by U-Th method and occurred from 221 ka to 190 ka and from 134 to 114 ka (Vaks et al, 2010). Earlier periods of deposition were dated by the U-Pb method on ASH-15 flowstone ~~and are dated to~~ 1.272 ± 0.018 Ma (ASH-15-C), and the Basal layer of ASH-15 flowstone (layers D-K) ~~dated to~~ c. ~3.1 Ma (Fig 1a). These layers have been dated in three different labs following several protocols for ID analysis (Vaks et al., 2013; Mason et al., 2013). The U concentrations in speleothem calcite range between 1.9 and 19.7 μg/g and the amounts of non-radiogenic Th are negligible (Vaks et al., 2010).

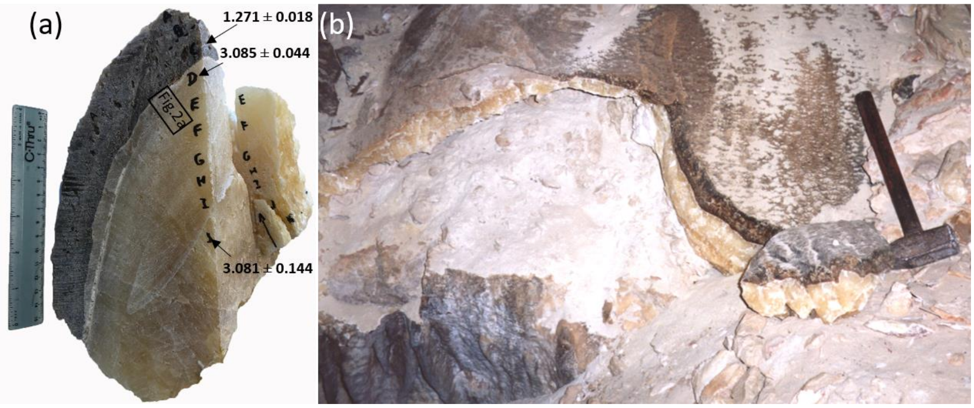

Figure 1. Sample ASH-15 from Ashalim Cave. (a) ~5 kg block of sample ASH-15 flowstone consisting of the massive Pliocene yellow Basal layer (>2 cm calcite crystals; section D–K) and the brown Quaternary layer (top section, A–C), the thin layer between the two stratigraphic members represents a growth break (hiatus). The main U-Pb ages of Vaks et al., 2013 are indicated. In-situ flowstone within Ashalim Cave from which ASH-15 was sampled, showing the large reservoir of this flowstone.

3. Sample ASH-15 textural characterization

The ASH-15 thin-section includes section D and E ~~of the ASH-15 sample~~ (see location in Fig.1a). Overall the thin-section examination indicates that the original texture is preserved with consistent growth direction, no observed hiatus, and no indications for dissolution and recrystallization. A spot analysis array, 85 µm in diameter, targeted along growth bands and perpendicular to growth ~~are~~ visible in Fig. 2a-c. The ASH-15 sample shows no luminescence under cathodoluminescence light (Fig. 2c), suggesting formation under oxidising conditions. The slight bright luminescence observed within grain boundaries, discontinuities, and veins (arrows in Fig. 2b-c) may suggest ~~for~~ the presence of fluid inclusions, textural differences, or some local replacement within these areas. These areas should be avoided if possible during spot analysis. The relatively homogenous low luminescence may suggest for a single-phase continuous calcite growth, whereby precipitation occurred relatively rapid from the same fluid source (e.g. with consistent Mn^{2+} Fe^{2+} composition) and/or under similar precipitation redox conditions. This 15 cm thick, ~3 Ma Pliocene layer (section D-K) is essentially of the same age. For this reason, previous dating of this sample also considered a similar initial $^{234}U/^{238}U$ activity ratio for disequilibrium correction (Mason et al., 2013; Vaks et al., 2013). The ASH-15 reference material consists of the whole Pliocene section that terminates with a sharp transition to the darker Pleistocene layers above it (section A-C; see Fig. 1b). About 3 kg of ASH-15 sample are excavated from the Ashalim Cave (Fig. 1a), and potentially much more can be sampled in the future (we estimate more than 10 kg of sample; Fig. 1b). The ASH-15 flowstone is therefore a good candidate for a reference material because of its large volume, high U concentrations, and potentially homogenous age which will be examine next.

https://doi.org/10.5194/gchron-2020-22
Preprint. Discussion started: 27 July 2020

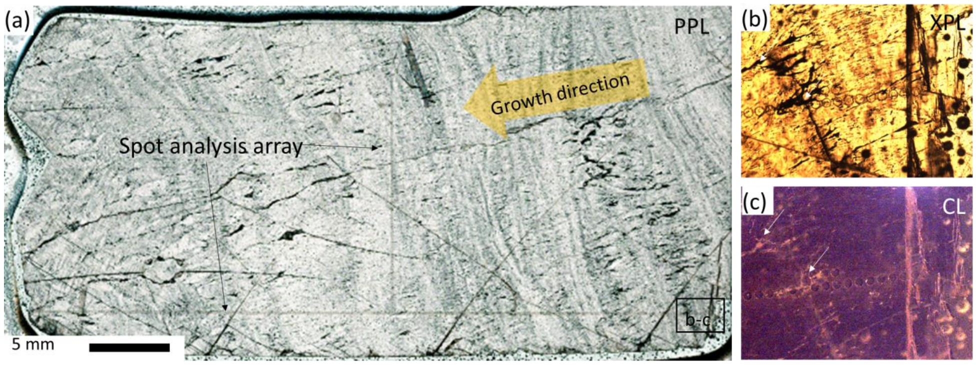

Figure 2. ASH-15D-E thin-section. (a) cross-polarized scan ~~of ASH-15D-E thin-section~~, 36 mm long, showing continuous growth (no hiatus), and consistent growth direction (indicated with yellow arrow). Spot analyses are targeted either parallel to growth band or perpendicular to growth direction~~,~~; (b) close-up on spot analyses (location is shown in a) with 85 µm diameter; (c) CL image of the same area showing no luminescence ~~and~~ some bright luminescence within grains boundaries and veins (arrows).

4. Methods

4.1. Elemental mapping

The sample ASH-15 was cut perpendicular to the growth bands of section D and E (see Fig.1b) in order to examine heterogeneities across growth bands and within. Thin-sections were then examined under plane- and cross-polarized light (XPL/PPL), and cathodoluminescence (CL) microscopy (Fig. 2). The central part of the thin-section was also analyzed for elemental distribution of selected elements. The elemental maps were measured via LA-ICPMS, carried out on a 193 nm ArF excimer laser ablation system (Analyte G2 Teledyne Photon Machines Inc., Bozeman MT) coupled to an ICP-QMS (Agilent 7900, Agilent Technologies, Santa Clara CA). The laser was equipped with a Photon Machines HelEx II ablation chamber and an Aerosol Rapid Introduction System (ARIS). The experiments were carried out using acquisition parameters (both on the ICP and on the laser) modelled using the approach of van Elteren et al (2019; 2018) to avoid artefacts (e.g., aliasing, smear, blur). All images (500x500 pixels) were acquired using a 20 µm square beam, fluence of 3.5 Jcm^{-2}, 294 Hz repetition rate and dosage of 10 (amounting to a scanning speed of 588 µms^{-1}). The masses monitored were ^{24}Mg, ^{55}Mn, ^{63}Cu, ^{85}Rb ^{88}Sr, ^{137}Ba, ^{206}Pb, ^{208}Pb, ^{232}Th, and ^{238}U and the images were constructed using Photon Machines' HDIP data reduction software (van Malderen, 2017).

4.2. LA-MC-ICPMS spot analyses

A thin section of ASH-15 was dated by U-Pb laser ablation multi-collector inductively coupled plasma mass spectrometry (LA-MC-ICPMS) following the method described in Nuriel et al. (2017). A Nu Plasma 3D was employed in conjunction with a Photon Machines Excite 193nm Excimer laser equipped with a HelEex two volume cell. The laser was fired for 15 s during analysis, using a rep rate of 10 Hz, a spot size of 85 µm, and a fluence of approx. 1 J/cm^2. The Nu Plasma 3D allows for the simultaneous acquisition of ^{238}U, ^{235}U, ^{232}Th, ^{208}Pb, ^{207}Pb, ^{206}Pb, ^{204}Pb(+Hg), and ^{202}Hg, where ^{238}U-^{232}Th are measured on Faraday detectors and the low-side masses are measured on Daly detectors. Instrumental mass-bias was corrected using a two-step approach: both the ^{207}Pb/^{206}Pb and ^{206}Pb/^{238}U ratios were first corrected to NIST-614 glass reference material in *Iolite 3* using the geochronology reduction scheme (Paton et al., 2010) to account for both mass-bias (^{207}Pb/^{206}Pb) and instrumental drift (^{207}Pb/^{206}Pb and ^{206}Pb/^{238}U). The Tera-Wasserburg data, output from *Iolite*, was then plotted and ^{206}Pb/^{238}U ratios of all RMs and unknowns were adjusted such that the primary calcite reference material—WC-1—yielded an age of 254 Ma (Roberts et al., 2017). This resulted in accurate dates for both our secondary calcite RM, Duff Brown Tank (64 Ma; Hill et al., 2016) and a zircon RM (Sri Lanka, 564 Ma; Gehrels et al., 2008), o[illegible].8 ± 3.4 Ma and a ^{207}Pb/^{206}Pb date of a 566.0 ± 2.8 Ma. Uncertainty propagation of individual ratios was assessed by reproducibility of the NIST614 and SL RMs (n=44 in both cases) and added in quadrature such that the MSWD of each weighted average is ≤1 and that the uncertainty is no better than 2% (long-term reproducibility); this resulted in propagated uncertainties of 2.5% and 2% for the ^{206}Pb/^{238}U and ^{207}Pb/^{206}Pb ratios, respectively. Given that the typical uncertainties of the ^{206}Pb/^{238}U and ^{207}Pb/^{206}Pb ratios of the unknowns was >10% and >3%, respectively, the uncertainty propagation on individual ratios had little effect on the calculation of the final date of ASH-15. The thin section of ASH-15 was measured both parallel to the length of section (303 spots, and perpendicular to it (101 spots). Data are plotted using Isoplot (Ludwig, 1998).

4.3. LA-ICPMS spot analyses

Analyses were conducted at the Geochronology and Tracers Facility, British Geological Survey (Nottingham, UK). The instrumentation comprised a New Wave Research 193UC excimer laser ablation system fitted with a TV2 cell, coupled to a Nu Instruments Attom single collector inductively coupled plasma mass spectrometer (ICP-MS). The method follows the protocols described in Roberts and Walker (2016) and Roberts et al. (2017). Laser parameters varied slightly per session, but typically involve a pre-ablation cleaning spot of 150 µm, fired at 10 Hz with a fluence of ~6 J/cm^2 for 2 seconds, and ablation conditions of 80-100 µm spots, fired at 10 Hz with a fluence of ~6-8 J/cm^2 for 25-30 seconds. A 60 second background is taken before every set of standard-bracketed analyses, and a 5 second washout is left between each ablation. Normalization of Pb-Pb ratios is achieved using NIST614 glass (values of Woodhead and Hergt, 2001), and WC-1 carbonate for Pb-U ratios (Roberts et al., 2017). Data reduction uses the Time Resolved Analysis function of the Nu Instruments Attolab software, and an excel spreadsheet, with uncertainty propagation following the recommendations of Horstwood et al. (2016).

4.4. ID-TIMS U-Pb geochronology

Isotope dilution thermal ionization mass spectrometry (ID-TIMS) U-Pb geochronology was performed at the Institute of Geochemistry and Petrology of ETH Zurich (ETHZ) and at the Department of Earth Sciences of the University of Geneva (UNIGE). Millimeter-sized chips of the ASH-15-D and ASH-15-K calcite were extracted using stainless steel tools. Larger chips were further sub-divided resulting in ~1-7 mg aliquots. Individual chips were transferred into 3 ml Savillex beakers and repeatedly ultrasonically cleaned in ultrapure acetone and water. Cleaned sampled were transferred into pre-cleaned 3 ml Savillex beakers, spiked with ~5-10 mg EARTHTIME (^{202}Pb-)^{205}Pb-^{233}U-^{235}U tracer solution (Condon et al., 2015) and dissolved in 6N HCl at 120°C on a hotplate for ~30 minutes to assure complete dissolution and sample-spike equilibration. Dissolved samples were dried down and redissolved in 1N HBr. Uranium and Pb were separated using a single-column (50 µl, AG1-X8 resin) HBr-HCl anion exchange chemistry. The Pb fraction was dried down with a drop of H_3PO_4 after a single column pass. Uranium was dried down, redissolved in 3N HCl and further purified with a HCl-based second column pass before drying it down with a drop of H_3PO_4. Uranium and Pb were loaded on outgassed single Re filaments with ~1 µl of Si-gel emitter for thermal ionization mass spectrometry. Uranium and Pb isotope ratios were measured on a Thermo TRITON Plus at ETHZ and a Thermo TRITON at UNIGE. Lead isotopes were measured on the axial secondary electron multiplier employing dynamic peak-hopping routine collecting masses (202), 204, 205, 206, 207 and 208. Measured Pb isotope ratios were corrected for mass fractionation either using the double spike (ETHZ) or using a mass fractionation factor of 0.15 ± 0.03 %/amu for single Pb spiked samples (UNIGE). Uranium isotope ratios were measured as uranium-oxide (UO_2) employing a static measurement routine with Faraday cups connected to amplifiers with 10^{13} ohm feedback resistors (von Quadt et al., 2016; Wotzlaw et al., 2017). Isotope ratios were corrected for isobaric interferences from minor UO_2 isotopologues (Wotzlaw et al., 2017) and for mass fractionation using the double spike assuming a $^{238}U/^{235}U$ ratio of 137.818 ± 0.045 (Hiess et al., 2012) for sample and blank. Total procedural Pb blanks for the HBr-based chemistry at ETHZ are consistently between 0.2 and 0.4 pg. We therefore attribute up to 0.4 pg to laboratory blank with the remaining common Pb being attributed to initial common Pb. Total procedural blanks measured at UNIGE yielded an average of 1.15 pg that was taken as the laboratory blank contribution. Data reduction and uncertainty propagation was performed using Tripoli and an Microsoft Excel-based spreadsheet that uses the algorithms of Schmitz and Schoene (2007). Isochron calculations were performed using IsoplotR (Vermeesch, 2018). All uncertainties are reported at 95% confidence ignoring systematic uncertainties associated with the tracer calibration and decay constants unless otherwise stated.

5. Results

All analyses were performed on ASH-15-D-K yellow Pliocene layer, abbreviated here as "ASH-15" unless specification of ASH-15-D, E etc. is indicated. The ASH-15-A-C brown Pleistocene layer is not part of the ASH-15 suggested reference material.

5.1. LA elemental mapping

Elemental mapping for ^{88}Sr, ^{137}Ba, ^{206}Pb, ^{208}Pb, ^{238}U and $^{238}U/^{206}Pb$ ratio shows that the distribution of most elements is relatively homogeneous (Fig.3), and in good accordance with the luminescence data. Higher intensities for ^{238}U and ^{88}Sr were observed along grain boundaries and discontinuities, whereas Pb and the rest of the trace elements are more homogeneously distributed arguing for environmental conditions ~~that have kept steady~~ during the deposition. Ten random regions of interest (ROI) were selected throughout the sample to mimic 10 spot analysis carried out at 85-90 microns spot size – just like one would do for U-Pb geochronology, ~~for example~~. These ROIs were generated by drawing on the map circular regions with the radius of 85 or 90 microns in diameter. The pixels comprising each ROI were pooled together as representing the equivalent of a single spot analysis. The statistical data for each cluster (data are given in supplementary file) ~~was~~ compared. The average values for all pixel data ~~is~~ within 2 standard errors and in good agreement, indicating that at least based on the elemental distribution we measured, the sample is relatively homogeneous for a natural sample. To further investigate the chemical homogeneity of the sample, a random transect through one of the growth zones was drawn and the signal intensities for ^{238}U were extracted. The transect data also indicate that ^{238}U variations are within 2 standard errors of the average value.

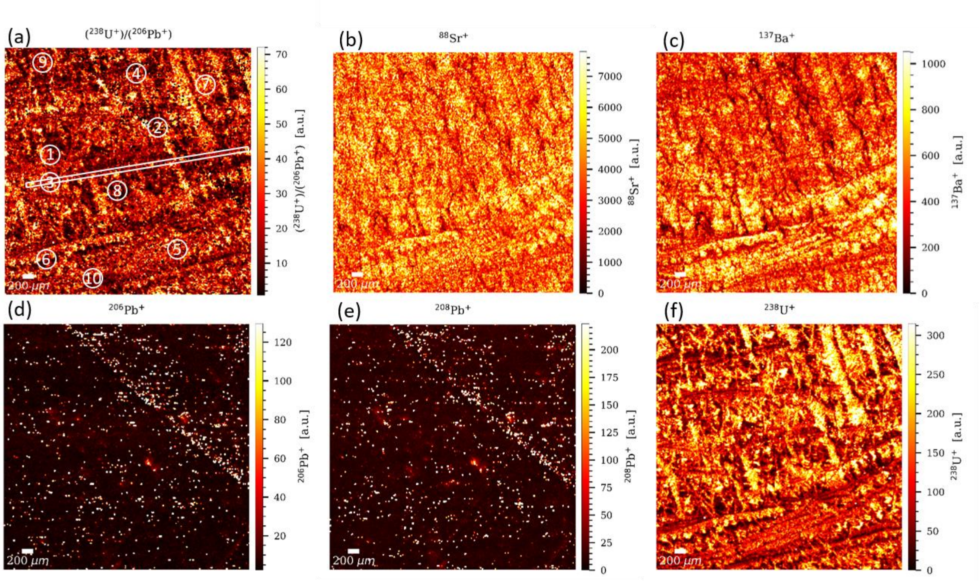

Figure 3. Signal intensity maps of ASH-15. for ^{238}U/^{206}Pb, ^{88}Sr, ^{137}Ba, ^{206}Pb, ^{208}Pb, and ^{238}U (a-d). The plotted signal was corrected for blank and analytical drift of the instrumentation. Note that each distribution map has its own signal intensity scale. The position of the regions of interest and transect is shown in (a). The circles designating the location of the regions of interest are not at scale.

5.2. LA-MC-ICPMS spot analyses

Data and calculated ages for the LA-ICPMS transects are shown in Tera-Wasserburg space in Fig. 4 (n = 379 of 412 total spots). Analyses rejected from the age calculation include those with ^{207}Pb/^{206}Pb uncertainties larger than 0.[illegible] ([illegible] = 2) and those with high common-Pb contents (^{208}Pb cps >5000; n = 17). A further 14 spots plotted below the array; these data ~~were~~ the first 1–2 mm of spots of the lengthwise transect (lower right in Fig. 2a), and suggest that a small percent of ASH-15 may behave differently during ablation and/or may have been subsequently modified after crystallization; upon inspection, this portion of the section contains more pore space and impurities than the majority of the section. The remaining 379 define a normally distributed array with a lower intercept age of 2.952 ± 0.043 Ma (MSWD = 2.5), which is well within uncertainty of the new ID-TIMS data presented ~~herein and the scatter observed in the LA data (i.e., MSWD > 1) is lower compared wi[illegible]catter observed in the ID-TIMS data.~~ The calculated upper intercept of each transect is equivalent and within 1% of the common Pb composition calculated from the ID-TIMS data. Not surprisingly, the lengthwise transect reveals a larger spread in common/radiogenic Pb ratios; this transect crosses more growth zones and has a higher probability of sampling a variety of concentrations of both Pb and U. Conversely, the more limited spread in common/radiogenic Pb ratios appears to reflect the limited sampling of growth zones, and would suggest that individual growth zones contain a relatively limited range of concentrations in U and Pb. The slightly higher MSWD for the lengthwise transect (2.7) relative to the growth zone transect (2.5) could also reflect these inherited compositional differences during growth history, and a ~~resulted~~ "mixing" or "averaging" of different growth phase along calcite continuous growth.

Variations of ASH-15 ages during 20 differ[illegible]uns using both single (ICPMS) and multi-collector (MC-ICPM) are shown in Fig. 4b. The ages are calculated using IsoplotR, anchored to 0.8315 common-lead, and are not corrected for disequilibrium. Although there is a large scatter in the ages of the different runs the average ages (marked in thick lines) ~~are~~ plot~~ted~~ close to the new ID-TIMS ages, or slightly younger in age.

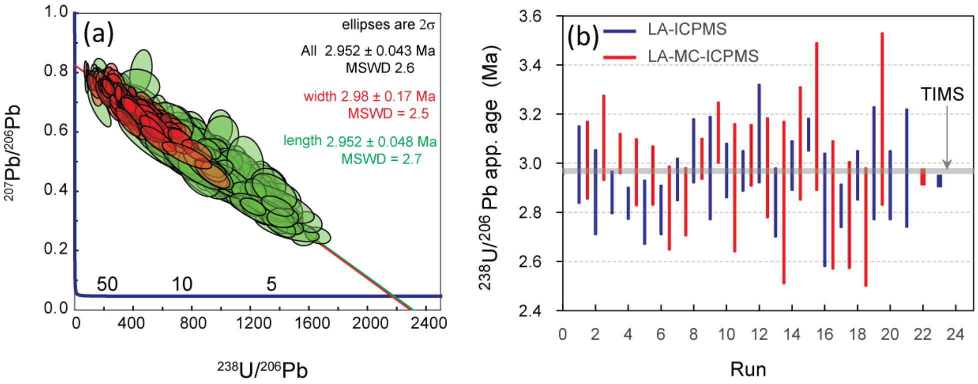

Figure 4. LA-MC-ICPMS analyses of calcite ASH-15 (n=385). Spots within lengthwise transect (green) and along growth zone transect (red). Calculated age, 2σ error and MSWD are given for both and for all spots together; (b) Variations of ASH-15 ages during different runs using both single and multi-collector ICPMS. Ages are calculated using WC1 as primary MS; the new ID-TIMS age is indicated with a grey line; Ages are calculated using IsoplotR, anchored to 0.8315 common-lead, and are not corrected for disequilibrium.

5.3. Down-hole fractionation

Reference material is important for correction of both laser-induced elemental fractionation (LIEF) and ~~in~~ plasma-related ionization efficiency. Ideally, the reference material should resemble the unknown samples as much as possible in terms of its chemistry (e.g. Mg and Fe content), texture (i.e. micritic, crystalline), and age. The WC1 and ASH15 are both low-Mg calcite but they are very different in ~~their~~ textures and age. The ASH15 is a ~3 Ma, well-crystallized elongated calcite (up to 1 cm) and WC1 is a 254 Ma recrystallized botryoidal calcite, formed after aragonite. Despite these differences, both WC1 and ASH15 display a very similar down-hole fractionation pattern (Fig. 5d). Fig. 5 shows stacked integration plots

https://doi.org/10.5194/gchron-2020-22
Preprint. Discussion started: 27 July 2020

of the down-hole raw $^{206}Pb/^{238}U$ ratio of different RMs including, the ASH15, WC-1, and Duff Brown Tank (Black and Gulson, 1978). The ASH15 display much larger scatter in the raw data (Fig. 5a) in comparison to both WC1 and Duff Brown Tank (Fig. 5b-c), however, the average value yielded identical down-hole patterns to that of WC-1 (Fig. 5d). Duff Brown Tank is also consistent with the down-hole patterns but less steep in comparison to WC1 and ASH15 (Fig. 5d). This comparison suggest that down-hole fractionation and laser-induced elemental fractionation (LIEF) ~~is~~ similar among the different RMs. It is thus suggested that differences in $^{206}Pb/^{238}U$ ratios ~~between measured and expected~~ in calcite material are likely to be caused mostly by plasma-ionization differences between unknown samples and RMs.

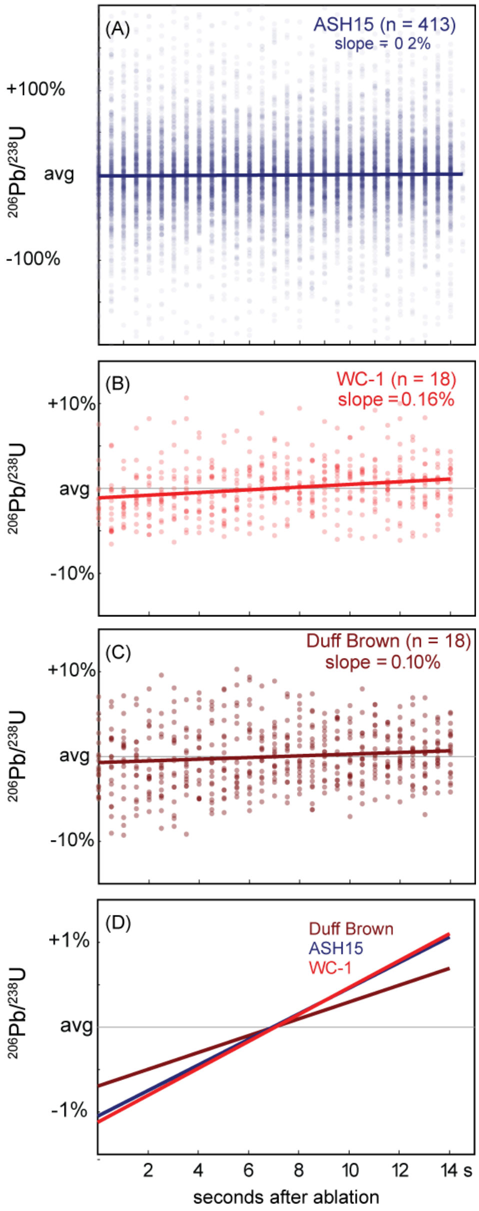

Figure 5. Stacked integration plots of raw ^{207}Pb-corrected ^{206}Pb/^{238}U ratios for calcite reference materials ASH-15, WC-1, and Duff Brown Tank. The low Pb concentration in ASH-15 yields more scatter, but average slopes of all RMs are similar, with 1-2% change in age over 10 seconds (100 pulses) of ablation. The results suggest ~~for~~ minimal differences in down-hole fractionation of the different RMs.

5.4. High-precision ID-TIMS results

Twelve aliquots of ASH-15D analyzed at ETHZ yielded $^{238}U/^{206}Pb$ ratios between 1096 and 2084 and $^{207}Pb/^{206}Pb$ ratios between 0.0825 and 0.4403. Plotted in Tera-Wasserburg space, ~~this~~ data yields a single isochron with an initial $^{207}Pb/^{206}Pb$ of 0.832 ± 0.015 (uncertainties are 95% confidence intervals) and a concordia intercept age of 2.967 ± 0.022 Ma (Fig. 6a). The elevated mean square weighted deviation (MSWD) of 12 is attributed to minor heterogeneities, most likely in the initial $^{207}Pb/^{206}Pb$ ratio of the speleothem calcite. Twelve aliquots of ASH-15K analysed at ETHZ returned $^{238}U/^{206}Pb$ ratios between 723 and 2094 and $^{207}Pb/^{206}Pb$ ratios between 0.0720 and 0.5677. In Tera-Wasserburg space, eleven out of twelve aliquots define a isochon with an initial $^{207}Pb/^{206}Pb$ of 0.8314 ± 0.0040 and a concordia intercept age of 2.964 ± 0.016 Ma (Fig. 6b). A single aliquot (#5.4) plots significantly below the isochron defined by the other aliquots. The elevated MSWD of 34 together with the single outlier suggest some heterogeneities in the initial $^{207}Pb/^{206}Pb$ of the ASH-15K calcite. Thirteen aliquots of ASH-15K analysed at UNIGE (pink color, Fig. 6b) yielded $^{238}U/^{206}Pb$ ratios between 433 and 1853 and and $^{207}Pb/^{206}Pb$ ratios ranging from 0.1856 to 0.6660. Twelve of the thirteen analyses yield define an isochron with an initial $^{207}Pb/^{206}Pb$ of 0.814 ± 0.019 and a Concordia intercept age of [illegible]7 ± 0.065 Ma. The elevated MSWD of 36 confirms the minor heterogeneity of the initial $^{207}Pb/^{206}Pb$.

The excellent agreement between the ASH-15D and ASH-15K datasets ~~suggest~~ that the entire speleothem growth layer between these two growth zones is of equivalent age with minor heterogeneities in the initial $^{207}Pb/^{206}Pb$ ratio and justifies combining the data into a single isochron regression. The combined isochron, using 35 of 37 analysed aliquots, yields an initial $^{207}Pb/^{206}Pb$ of 0.8306 ± 0.0033 and a concordia intercept age of 2.965 ± 0.011 Ma with a MSWD of 35 (Fig. 6c). We consider the results of the combined ~~isochron~~ regression as the best reference value for using ASH-15 as a primary reference material.

The new TIMS data provide the most extended ~~bulk-analyses work~~ of the ASH-15 sample, with a total of 37 sub-samples that are separated from bottom (K, n=25) to top (D, n=12) ~~sections of the sample~~. The ~~relatively~~ high MSWD of 35 is suggested to reflect true heterogeneities of the dated material, possibly related to impurities that are concentrated within grain boundaries (as suggested by CL and elemental mapping). We re-calculated previously determined isochron ages of Vaks et al. (2013) and Mason et al. (2013; Fig. 7). We obtained concordia intercept ages of 3.0088 ± 0.053 Ma for ASH-15-D (MSWD=11; n=5) and 3.0153 ± 0.042 Ma for ASH-15-K (MSWD=14; n=5) of Vaks et al. (2013) and 3.0015 ± 0.029 for ASH-15-D (MSWD=2; n=5) of Mason et al. (2013). These ages are systematically older but still overlap within uncertainty with our new age of 2.965 ± 0.011 Ma (Fig. 7). We speculate that the ~~small but~~ systematic offset between previous results and our new data may be related to natural heterogeneities that are sampled differently depending on sample size but we cannot exclude analytical differences as an additional source of bias. The origin of this bias between the two techniques should be investigated more systematically in future. For laser ablation U-Pb work, we recommend the use of the new ID-TIMS age because of the large number of sub-samples (n=37), and the small aliquots (1-7 mg) that are more representative of laser-ablation spot analysis. In addition, the use of the precisely and accurately calibrated EARTHTIME tracer solutions (Condon et al., 2015) and the online mass fractionation correction provided by the double Pb and double U tracer are an important advantage of this method compared to previous bulk analyses. The excellent interlaboratory reproducibility gives us additional confidences that our ID-TIMS data provide the most accurate characterization of the U-Pb systematics of the ASH-15 calcite for use as a primary reference material.

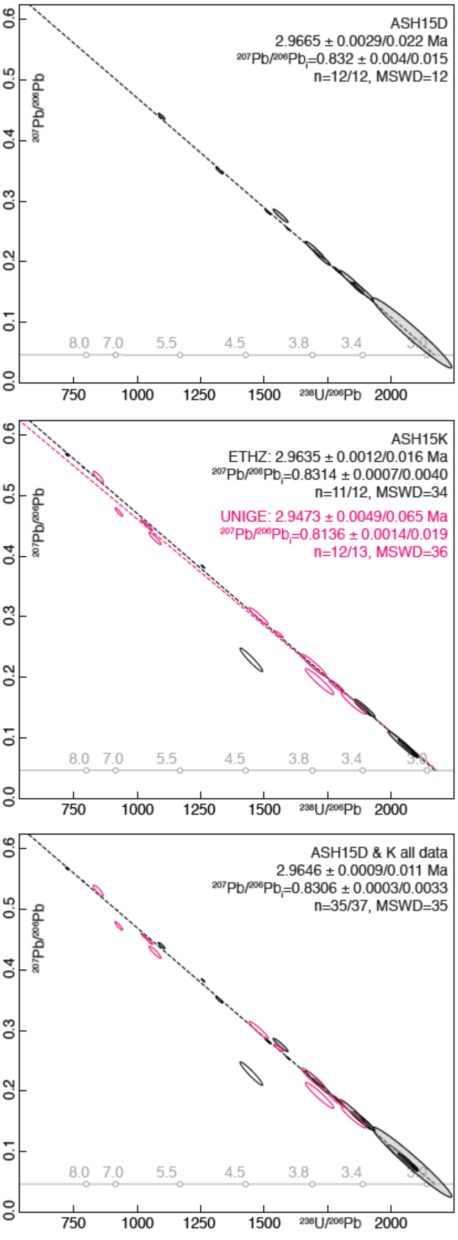

Figure 6. ID-TIMS U-Pb results for ASH-15D, ASH-15K, and for both ASH-15D +K.

https://doi.org/10.5194/gchron-2020-22
Preprint. Discussion started: 27 July 2020

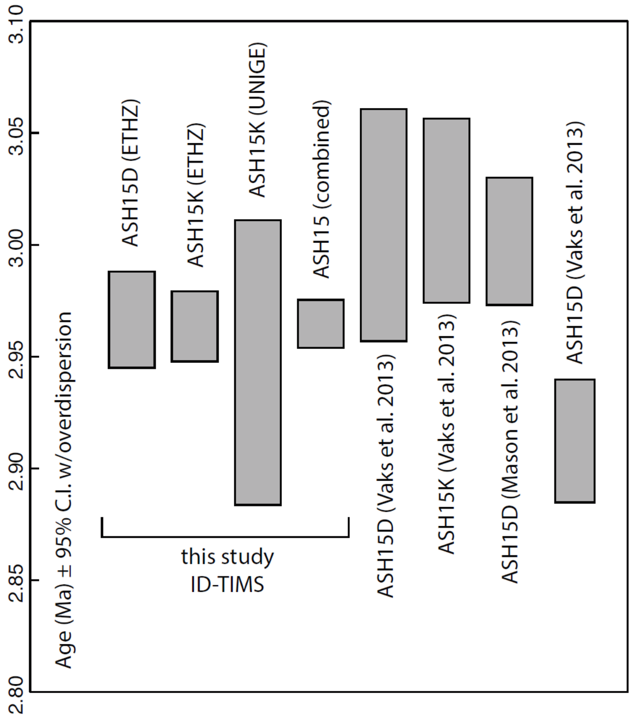

Figure 7. Previous (re-calculated) and new ages of ASH-15 from isotope-dilution U-Pb analysis. All ages are calculated using IsoplotR ~~and~~ are not corrected for disequilibrium and are not anchored to common-lead specific value.

6. Conclusions

The ASH-15 speleothem calcite is characterized as a matrix matched reference material for LA-ICPMS U-Pb geochronology of calcite. ID-TIMS analyses of small 1-7 mg aliquots of two growth zones suggest sufficient homogeneity with a combined intercept age of 2.965 ± 0.011 Ma and an initial ^{207}Pb/^{206}Pb of 0.8315 ± 0.0026. These data are recommended as the reference values for the ASH-15 calcite reference material. The excellent agreement between the two growth zones suggest that the entire interval between the two dated layers can be used with the same reference age. Compared to other calcite reference material (e.g. WC1), ASH-15 is more homogeneous but has lower radiogenic Pb content and therefore requires more sensitive instruments (i.e. sector field rather than quadrupole mass spectrometers) to be used as a reference material.

Table 1. U-Th-Pb isotopic data

Sample (a)	Wt. mg (b)	U ppm (c)	Pb ppm (c)	Th/U (d)	^{206}Pb* x10^{-13} mol (e)	mol % ^{206}Pb* (e)	Pb*/Pbc (e)	Pbc (pg) (e)	^{206}Pb/^{204}Pb (f)
ASH-15D (ETHZ)									
2	2.165	2.24	0.002	0.009	0.0931	82.28%	1.23	1.63	105
3	2.392	1.26	0.001	-	0.0569	66.53%	0.52	2.34	56
5	4.085	1.80	0.001	0.010	0.1409	80.14%	1.07	2.85	94
6	5.446	1.99	0.002	0.020	0.2110	73.23%	0.73	6.31	70
8	3.994	1.90	0.002	0.018	0.1466	68.61%	0.58	5.49	60
10	1.523	2.15	0.002	-	0.0625	80.81%	1.10	1.21	97
11	1.600	1.70	0.001	0.015	0.0519	78.34%	0.96	1.17	86
12	0.965	1.18	0.001	0.039	0.0218	78.32%	0.98	0.48	85
13	1.776	1.95	0.002	0.022	0.0666	75.21%	0.81	1.79	75
14	2.470	1.90	0.003	0.022	0.0908	59.47%	0.39	5.06	46
16	1.827	1.65	0.003	0.014	0.0577	48.13%	0.25	5.09	36
17	1.680	1.96	0.002	0.011	0.0632	73.55%	0.74	1.85	71
ASH-15K (ETHZ)									
3.1	3.025	9.94	0.025	0.033	0.5834	42.70%	0.20	64.16	33
3.2	1.313	2.56	0.009	0.025	0.0662	33.30%	0.13	10.86	28
4.1	3.200	2.62	0.008	-	0.1632	36.38%	0.15	23.39	29
5.1	3.662	2.28	0.004	0.036	0.1593	56.52%	0.35	10.04	43
5.2	2.229	1.17	0.001	0.019	0.0504	86.50%	1.72	0.63	138
5.3	1.548	2.13	0.002	0.030	0.0631	81.40%	1.17	1.17	100
5.4 (j)	*1.221*	*1.42*	*0.002*	*0.021*	*0.0383*	*69.98%*	*0.62*	*1.34*	*62*
7.1	2.108	2.47	0.001	-	0.1003	90.66%	2.58	0.84	199
7.2	2.595	2.94	0.002	0.010	0.1467	92.03%	3.08	1.03	234
9.1	3.125	1.30	0.001	0.000	0.0778	82.46%	1.25	1.35	106
10.1	2.525	4.77	0.002	0.008	0.2327	94.93%	4.99	1.01	367
10.2	3.269	3.25	0.002	0.003	0.2039	94.08%	4.23	1.04	314
ASH15K (UNIGE)									
2.1	3.3	0.43	0.003	-	0.0293	19.59%	0.06	9.86	23
2.2	2.0	3.83	0.003	-	0.1483	79.60%	1.02	3.11	91
2.4 (j)	*4.5*	*3.12*	*0.016*	*-*	*0.2031*	*18.93%*	*0.03*	*71.29*	*23*
2.5	2.1	2.67	0.003	-	0.1108	73.96%	0.74	3.20	72
6.1	2.5	2.47	0.003	-	0.1184	71.35%	0.64	3.90	65
6.2	7.3	2.38	0.003	-	0.3346	69.67%	0.60	11.94	62
6.3	2.8	2.25	0.003	-	0.1207	62.96%	0.44	5.82	50
6.4	5.0	2.53	0.002	-	0.2440	78.69%	0.97	5.42	88
6.5	1.9	2.10	0.007	-	0.0761	36.09%	0.14	11.05	29
9.2	2.7	7.08	0.016	-	0.3746	47.26%	0.23	34.27	35
9.3	2.6	2.04	0.004	-	0.1063	48.13%	0.24	9.39	36
9.4	2.5	2.59	0.007	-	0.1347	44.10%	0.20	13.99	33
9.5	2.1	4.90	0.011	-	0.2012	47.43%	0.23	18.28	36

(a) Fractions are single chips of calcite

(b) mass of fraction in mg

(c) U and total Pb concentrations.

(d) Model Th/U ratio iteratively calculated from the radiogenic ^{208}Pb/^{206}Pb ratio and ^{206}Pb/^{238}U age.

~~Fractions without value (-) have ^{208}Pb/^{204}Pb indistinguishable from common Pb therefore no Th content was calculated~~.

(e) Pb* and Pbc represent radiogenic and common Pb, respectively; mol % ^{206}Pb* with respect to radiogenic, blank and initial common Pb.

(f) Measured ratio corrected for spike and fractionation only.

(g) Corrected for fractionation, spike, and blank Pb only.

(h) Errors are 2-sigma, propagated using the algorithms of Schmitz and Schoene (2007).

(g) Isochron age calculations are based on the decay constants of Jaffey et al. (1971).

(j) Fraction excluded from isochron regressions

Appendices

Figure A1. Photographs of ASH15 flowstone with layers D (light) and C (brown). Sampling localities of aliquots sampled for ID-TIMS analyses are indicated by numbers matching the aliquots in the data table. Larger pieces were chipped off using a stainless steel needle and subdivided into smaller aliquots for analysis.

Figure A2. Photographs of ASH15 flowstone with layers K (bottom) to D (top). Sampling localities of aliquots samples for ID-TIMS analyses within layer K are indicated with numbers (n=12) and are matching the aliquots in the data table.

References:

Anjiang, S., Anping, H., Cheng, T., Liang, F., Wenqing, P., Yuexing, F., and Zhao, J.: Laser ablation in situ U-Pb dating and its application to diagenesis-porosity evolution of carbonate reservoirs, 46, 1127-1140, 2019.

Condon, D., Schoene, B., McLean, N., Bowring, S., and Parrish, R.: Metrology and traceability of U–Pb isotope dilution geochronology (EARTHTIME Tracer Calibration Part I), Geochimica et Cosmochimica Acta, 164, 464-480, 2015.

Coogan, L. A., Parrish, R. R., and Roberts, N. M.: Early hydrothermal carbon uptake by the upper oceanic crust: Insight from in situ U-Pb dating, Geology, 44, 147-150, 2016.

Crouvi, O., Amit, R., Enzel, Y., and Gillespie, A. R.: Active sand seas and the formation of desert loess, Quaternary Science Reviews, 29, 2087-2098, 2010.

Godeau, N., Deschamps, P., Guihou, A., Leonide, P., Tendil, A., Gerdes, A., Hamelin, B., and Girard, J.-P. J. G.: U-Pb dating of calcite cement and diagenetic history in microporous carbonate reservoirs: Case of the Urgonian Limestone, France, 46, 247-250, 2018.

Guillong, M., Wotzlaw, J. F., Looser, N., and Laurent, O.: New analytical and data evaluation protocols to improve the reliability of U-Pb LA-ICP-MS carbonate dating, Geochronology Discuss., 2020, 1-17, 10.5194/gchron-2019-20, 2020.

Hansman, R. J., Albert, R., Gerdes, A., and Ring, U.: Absolute ages of multiple generations of brittle structures by U-Pb dating of calcite, Geology, 46, 207-210, 2018.

Hiess, J., Condon, D. J., McLean, N., and Noble, S. R.: 238U/235U systematics in terrestrial uranium-bearing minerals, Science, 335, 1610-1614, 2012.

Holdsworth, R., McCaffrey, K., Dempsey, E., Roberts, N., Hardman, K., Morton, A., Feely, M., Hunt, J., Conway, A., and Robertson, A.: Natural fracture propping and earthquake-induced oil migration in fractured basement reservoirs, Geology, 47, 700-704, 2019.

Horstwood, M. S., Košler, J., Gehrels, G., Jackson, S. E., McLean, N. M., Paton, C., Pearson, N. J., Sircombe, K., Sylvester, P., and Vermeesch, P.: Community- derived standards for LA-ICP-MS U-(Th-) Pb geochronology–Uncertainty propagation, age interpretation and data reporting, Geostandards and Geoanalytical Research, 40, 311-332, 2016.

Li, Q., Parrish, R., Horstwood, M., and McArthur, J.: U–Pb dating of cements in Mesozoic ammonites, Chemical Geology, 376, 76-83, 2014.

Lisiecki, L. E., and Raymo, M. E.: A Pliocene-Pleistocene stack of 57 globally distributed benthic δ^{18}O records, Paleoceanography, 20, 2005.

MacDonald, J., Faithfull, J., Roberts, N., Davies, A., Holdsworth, C., Newton, M., Williamson, S., Boyce, A., John, C. J. C. t. M., and Petrology: Clumped-isotope palaeothermometry and LA-ICP-MS U–Pb dating of lava-pile hydrothermal calcite veins, 174, 63, 2019.

Mason, A. J., Henderson, G. M., and Vaks, A.: An Acetic Acid-Based Extraction Protocol for the Recovery of U, Th and Pb from Calcium Carbonates for U-(Th)-Pb Geochronology, Geostandards and Geoanalytical Research, 37, 261-275, 10.1111/j.1751-908X.2013.00219.x, 2013.

Nuriel, P., Weinberger, R., Kylander-Clark, A. R. C., Hacker, B. R., and Craddock, J. P.: The onset of the Dead Sea transform based on calcite age-strain analyses, Geology, *45*, 587-590, 10.1130/g38903.1, 2017.

Nuriel, P., Craddock, J., Kylander-Clark, A. R., Uysal, I. T., Karabacak, V., Dirik, R. K., Hacker, B. R., and Weinberger, R. J. G.: Reactivation history of the North Anatolian fault zone based on calcite age-strain analyses, 47, 465-469, 2019.

Parrish, R. R., Parrish, C. M., and Lasalle, S.: Vein calcite dating reveals Pyrenean orogen as cause of Paleogene deformation in southern England, Journal of the Geological Society, 10.1144/jgs2017-107, 2018.

Piccione, G., Rasbury, E. T., Elliott, B. A., Kyle, J. R., Jaret, S. J., Acerbo, A. S., Lanzirotti, A., Northrup, P., Wooton, K., and Parrish, R. R.: Vein fluorite U-Pb dating demonstrates post–6.2 Ma rare-earth element mobilization associated with Rio Grande rifting, Geosphere, 15, 1958-1972, 2019.

Ring, U., and Gerdes, A.: Kinematics of the Alpenrhein-Bodensee graben system in the Central Alps: Oligocene/Miocene transtension due to formation of the Western Alps arc, Tectonics, 35, 1367-1391, 10.1002/2015TC004085/abstract, 2016.

Roberts, N. M., and Walker, R. J.: U-Pb geochronology of calcite-mineralized faults: Absolute timing of rift-related fault events on the northeast Atlantic margin, Geology, 44, 531-534, 2016.

Roberts, N. M., Rasbury, E. T., Parrish, R. R., Smith, C. J., Horstwood, M. S., and Condon, D. J.: A calcite reference material for LA-ICP-MS U-Pb geochronology, Geochemistry, Geophysics, Geosystems, 2017.

Schmitz, M. D., and Schoene, B.: Derivation of isotope ratios, errors, and error correlations for U-Pb geochronology using ^{205}Pb-^{235}U-(^{233}U)-spiked isotope dilution thermal ionization mass spectrometric data, Geochemistry, Geophysics, Geosystems, 8, 2007.

Vaks, A., Bar-Matthews, M., Matthews, A., Ayalon, A., and Frumkin, A.: Middle-Late Quaternary paleoclimate of northern margins of the Saharan-Arabian Desert: reconstruction from speleothems of Negev Desert, Israel, Quaternary Science Reviews, 29, 2647-2662, 2010.

Vaks, A., Woodhead, J., Bar-Matthews, M., Ayalon, A., Cliff, R. A., Zilberman, T., Matthews, A., and Frumkin, A.: Pliocene–Pleistocene climate of the northern margin of Saharan–Arabian Desert recorded in speleothems from the Negev Desert, Israel, Earth and Planetary Science Letters, 368, 88-100, http://dx.doi.org/10.1016/j.epsl.2013.02.027, 2013.

Vaks, A., Bar-Matthews, M., Ayalon, A., Matthews., A., Frumkin, A. Pliocene – Pleistocene paleoclimate reconstruction from Ashalim Cave speleothems, Negev Desert, Israel., In: Parise, M., Gabrovsek, F., Kaufmann, G. & Ravbar, N. (eds) Advances in Karst Research: Theory, Fieldwork and Applications. Geological Society, London, Special Publications, 466 (1), pp. 201-206, 2018.

van Elteren, J. T., Šelih, V. S., Šala, M., Van Malderen, S. J., and Vanhaecke, F.: Imaging artifacts in continuous scanning 2D LA-ICPMS imaging due to nonsynchronization issues, Analytical chemistry, 90, 2896-2901, 2018.

van Elteren, J. T., Šelih, V. S., and Šala, M.: Insights into the selection of 2D LA-ICP-MS (multi) elemental mapping conditions, Journal of Analytical Atomic Spectrometry, 34, 1919-1931, 2019.

van Malderen, S.: Optimization of methods based on laser ablation-ICP-mass spectrometry (LA-ICP-MS) for 2-D and 3-D elemental mapping, Ghent University, 2017.

Vermeesch, P.: IsoplotR: A free and open toolbox for geochronology, Geoscience Frontiers, 2018.

von Quadt, A., Wotzlaw, J.-F., Buret, Y., Large, S. J., Peytcheva, I., and Trinquier, A.: High-precision zircon U/Pb geochronology by ID-TIMS using new 10 13 ohm resistors, Journal of Analytical Atomic Spectrometry, 31, 658-665, 2016.

Woodhead, J., and Petrus, J. J. G.: Exploring the advantages and limitations of in situ U–Pb carbonate geochronology using speleothems, 1, 69-84, 2019.

Woodhead, J. D., and Hergt, J. M.: Strontium, neodymium and lead isotope analyses of NIST glass certified reference materials: SRM 610, 612, 614, Geostandards Newsletter, 25, 261-266, 2001.

Wotzlaw, J.-F., Buret, Y., Large, S. J., Szymanowski, D., and von Quadt, A.: ID-TIMS U–Pb geochronology at the 0.1‰ level using 10 13 Ω resistors and simultaneous U and ^{18}O/^{16}O isotope ratio determination for accurate UO 2 interference correction, Journal of Analytical Atomic Spectrometry, 32, 579-586, 2017.